Journal of Materials Physics and Chemistry, 2024, Vol. 12, No. 3, 42-48
Available online at http://pubs.sciepub.com/jmpc/12/3/1
Published by Science and Education Publishing
DOI:10.12691/jmpc-12-3-1

Synthesis and Physicochemical Properties of Ordered Mesoporous $Mn_{0.6}Cu_{0.4}Co_2O_4$ as High-performance Bifunctional Electrode for Zn-Air Batteries

Sangaré Kassoum[1,*], Seyhi Brahima[2], Coulibaly Bamoro[1]

[1]Département des Sciences et Technologies Agro-Industrielles, UFR Agriculture, Ressources Halieutiques et Agro-Industrie, Université de San – Pédro, BP 1800, San – Pédro, Côte d'Ivoire
[2]Département de Géosciences, UFR des Sciences Biologiques, Université Péléforo Gon Coulibaly, BP 1328, Korhogo, Côte d'Ivoire
*Corresponding author: kassoum.sangare@usp.edu.ci

Received August 16, 2024; Revised September 18, 2024; Accepted September 24, 2024

Abstract The aim of the present study was to synthesize $Mn_{0.6}Cu_{0.4}Co_2O_4$ electrocatalyst powder using nanocasting method with KIT6-100 silica and to investigate its chemical and physicochemical properties. Nanocasting process induced high oxide specific surface areas to the electrocatalyst, with BET surface value of 132 m^2/g. By comparison, 91 m^2/g was obtained by the classic solgel method. Pore size distribution investigation revealed a mesoporous structuration of the electrocatalyst synthetized by nanocasting route. This led to uniform pore size of ca. 6.1 nm whereas, a large distribution from 2 to 50 nm was found for solgel method. The uniform and controlled pore size contributed to effective penetration of the liquid electrolyte. X-ray diffraction (XRD) study revealed spinel lattice structure with large crystallites of about 8 nm. X-ray photoelectron spectroscopy (XPS) measurements confirmed the presence of metal adsorption sites for electrocatalytic reactions. It also showed the predominance of Co^{2+}, Cu^{2+} and Mn^{4+} species at the sample's surfaces, beneficial for good intrinsic activities of oxygen reduction reaction (ORR) and oxygen evolution reaction (OER).

Keywords: *electrocatalyst, spinel structure, nanocasting, solgel, specific surface area, pore size*

Cite This Article: Sangaré Kassoum, Seyhi Brahima, and Coulibaly Bamoro, "Synthesis and Physicochemical Properties of Ordered Mesoporous $Mn_{0.6}Cu_{0.4}Co_2O_4$ as High-performance Bifunctional Electrode for Zn-Air Batteries." *Journal of Materials Physics and Chemistry*, vol. 12, no. 3 (2024): 42-48. doi: 10.12691/jmpc-12-3-1.

1. Introduction

In recent years, studies of various mixed (ternary and quaternary) oxides have increased their applicability to serve as suitable substitutes for noble metal catalysts in a variety of areas. Transition metal compounds have been of great interest due to their high theoretical capacity, rich reserves, low cost, stable in an alkaline environment and stable structure [1,2,3,4,5]. Many transition metal oxides structures have been studied, among which manganese/cobalt-based spinel-type oxides are particularly promising as bifunctional electrocatalysts [6,7,8,9]. De Koninck and *al.* have shown that the $CuCo_2O_4$ electrocatalyst has excellent properties for both oxygen reduction reaction (ORR) and oxygen evolution reaction (OER) in an alkaline medium [8,9,10]. They also noticed that the electrocatalytic activities for ORR and OER depend strongly on the manganese (Mn) content in $CuCo_2O_4$. Mn affects significant intrinsic and apparent electrocatalytic activities of both oxygen electrode reactions and the highest electrochemical activities were found for $Mn_{0.6}Cu_{0.4}Co_2O_4$. In this work, synthesis of bifunctional $Mn_{0.6}Cu_{0.4}Co_2O_4$ electrocatalyst powders for oxygen evolution and reduction reaction was carried out using classical solgel and nanocasting synthesis routs. The $Mn_{0.6}Cu_{0.4}Co_2O_4$ electrocatalyst powder was first characterized to ensure intrinsic properties such as stoichiometry, crystalline, micrograph structure, surface and element chemical state. Then, the porosity structure and BET surface area were evaluated by pore sized distribution and BET measurement, respectively.

2. Material and Methods

2.1. Chemicals

Chemical used, including Co $(NO_3)_2.6H_2O$, Cu $(NO_3)_2.3H_2O$, Mn $(NO_3)_2.4H_2O$, anhydrous ethanol, HNO_3, Pluronic P123, HCl, Tetraethoxysilane, NaOH, were of purity grade. They were purchased from Sigma-Aldrich Canada Ltd. (Oakville, ON, Canada). Stock solutions of Co $(NO_3)_2.6H_2O$, Cu $(NO_3)_2.3H_2O$, Mn $(NO_3)_2.4H_2O$ were

prepared in acidified anhydrous ethanol and used to prepare stoichiometric mixture of Co, Cu et Mn.

2.2. Synthesis of $Mn_{0.6}Cu_{0.4}Co_2O_4$ Electrocatalyst

$Mn_{0.6}Cu_{0.4}Co_2O_4$ electrocatalyst powder was synthesized using simple solgel method and nanocasting method. Solgel method start with the preparation of stoichiometric mixture of cobalt, copper and manganese precursors using stock solutions of Co $(NO_3)_2.6H_2O$ (0.364 M, 51.8 mL), Cu $(NO_3)_2.3H_2O$ (0.36 M, 12.2 mL) and Mn $(NO_3)_2.4H_2O$ (0.374 M, 15.3 mL). The xerogel were obtained after 4 h refluxed/stirring to ensure thermal hydrolysis. The solvent was evaporated from the xerogel at 40°C using a rotating evaporator (Rose Scientific Ltd.) and dried at 200°C under dry air during 10 h, ground in a mortar before annealing process at 350°C in air and atmosphere condition in a tubular furnace (Lindberg/Blue M, model TF55035A).

Nanocasting method was performed according to the protocol described by Kleitz et al. [11]. The xerogel obtained from the solgel method was mixed with 0.4 g of silica (KIT6-100). The KIT6-100 was prepared from 6 g de Pluronic P123 in 217 g of distilled/ deionized water, 11.8 g of HCL (35%) and 12.9 g de Tetraethoxysilane. The suspension was stirred 24 h to induce penetration of the particles into KIT6 100 pores and the product was dried and suspended in 1 M NaOH solution to remove the silica. The sample was dried at 200°C under dry air during 10 h, ground in a mortar and annealed in the same condition as previously.

2.3. Analytical Methods

Co, Cu and Mn were analyzed using an atomic spectrometer Varian SpectrAA 220FS (Varian, USA). Co (λ=240.7 nm), Cu (λ=324.8 nm) and Mn (λ=279.5 nm) lamps were used to carry out these analyzes. The scanning electron microscopy (SEM) has been performed on a Hitachi S-4300 SE/N (Hitachi, Japan). The semiquantitative chemical composition of the powders was determined by energy dispersive X-ray (EDX) analysis (EDX Detector, Sapphire) integrated into the SEM. X-ray photoelectron spectroscopy was performed on the XPS PHI 5600-ci spectrophotometer (Physical Electronics, Eden Prairie, MN, USA) equipped with a monochromatic aluminum source of 1486.6 eV at 300 W for overview spectra and a Mg, Kα anode of 1253.6 eV at 300 W for high-frequency spectra resolution (HR). The specific surface area of the electrocatalyst particles was obtained by measuring at 77 K the adsorption and desorption of N_2 using a Quantachrome autoadsorb-1 (Quantachrome Instruments, USA). The pore size distribution was evaluated using the DFT method. X-ray diffraction (XRD) of the sample was carried out using the Siemens D5000 diffractometer (Siemens, Germany). The crystallite size (t_{hkl}) of the oxide particles was calculated using the Debye-Scherrer formula according to Equation 1.

Equation 1. $$t_{hkl} = \frac{0.9\lambda}{\beta cos\theta}$$

Where h, k, and l are the Miller indices, λ is the wavelength of the cobalt source (17.890 nm), β is the width at half height in radians of the main diffraction peak (311), and θ is the diffraction angle of the selected peak (21.5°).

3. Results and Discussion

3.1. Chemicals Characterization of Mn0.6Cu0.4Co2O4

The micrographs of $Mn_{0.6}Cu_{0.4}Co_2O_4$ samples prepared by solgel and nanocasting routes are shown in Figure 1. They present the morphology and the surface structure of $Mn_{0.6}Cu_{0.4}Co_2O_4$ samples. It's clear that, the as-prepared electrocatalyst nanoparticles are agglomerated and exhibited aggregates and irregular morphology due to the calcination process [12].

The spectra of EDX analysis showed the presence of the several elements in the catalyst, such as O, Cu, Co, Mn and C (Figure 2). The average surface composition from the atomics ratios percentage (Table 1) was found to be $Mn_{0.6}Cu_{0.5}Co_2O_{3.6}$ in agreement with theoretically chemical formula of $Mn_{0.6}Cu_{0.4}Co_2O_4$. The weak peak of silica observed in nanocasting synthesis method (Figure 2b), shows the efficacity of the washed process using NaOH solution. This similar result have been reported when using other silica washing such boiling ethanol for 15 h [13].

Table 1. EDX atomic percentages (*At %*) of samples elements

Synthesis route	T (°C)	O (K)	Mn (L)	Co (L)	Cu (L)
Solgel	350	50.29	9.42	30.72	9.55
Nanocasting		39.26	6.89	24.39	4.44

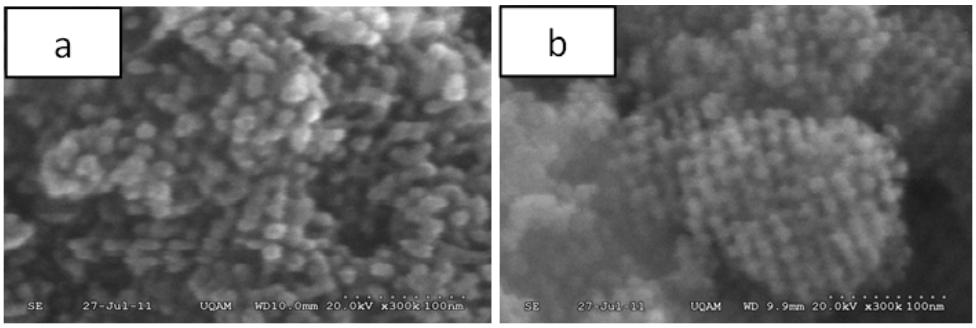

Figure 1. Micrographs of $Mn_{0.6}Cu_{0.4}Co_2O_4$ powders prepared by solgel (a) and nanocasting route (b) and annealed at 350 °C under atmosphere and air conditions

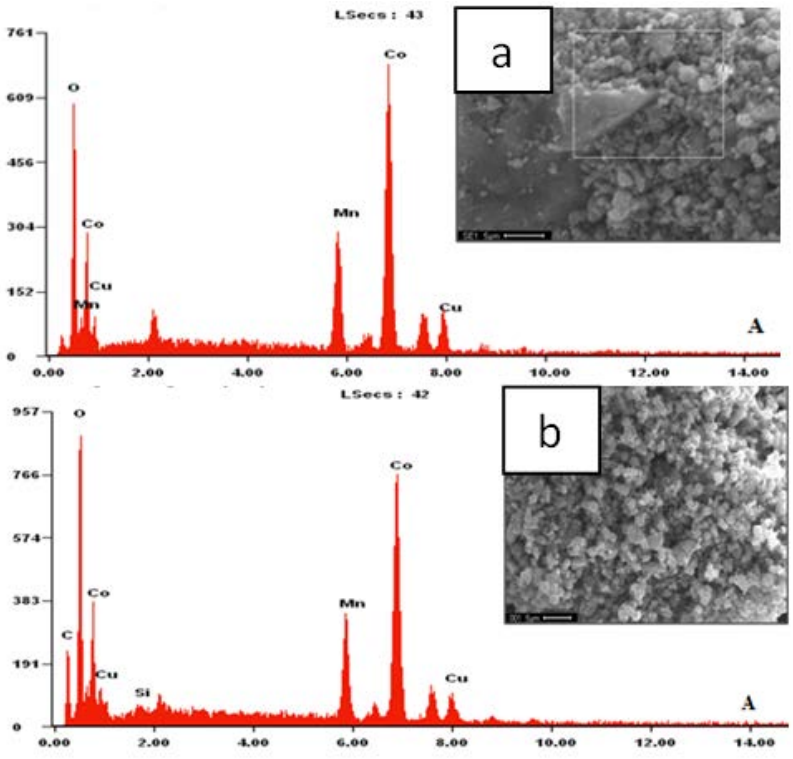

Figure 2. Typical EDX spectra and regions analyzed on the $Mn_{0.6}Cu_{0.4}Co_2O_4$ surface prepared by a) solgel, b) nanocasting route and annealed at 350 °C under atmosphere and air conditions

The surface elemental composition and the chemical states of various elements are shown in Figure 3. C1s peak at 284.6 eV, corresponding to contaminated carbon was used as reference. XPS spectra confirmed the presence of metals Mn, Cu, Co and O at the surface of the electrocatalyst. Metal favor ORR/OER reactions because of the availability of adsorption and desorption sites of species O_2, OH^-, $H_2O_2^-$ involved in these reactions [14,15,16,17]. Since method used for the synthesis of catalysts does not influence the XPS results, only results from nanocasting method are presented in this section.

The high-resolution photoelectron spectra of Co 2p is presented in Figure 4 and data related to the deconvolved peaks are shown in Table 2. Co 2p core-level spectrum shows different peaks, corresponding to Co 2p3/2 (~ 780.1 eV), Co 2p1/2 (~ 795.4 eV) and broad satellite peaks SI, SII, SIII [18]. The spin-orbit doublet of binding energy (BE ~ 779 and 794 eV) with ΔBE ~ 15 eV is characteristic of the Co^{3+} ion in octahedral sites [19], whereas the second doublet of binding energies (BE~ 780 and 795 eV) with ΔBE~ 15 eV is characteristic of the Co^{2+} ion in tetrahedral sites[19] . SI, SII, SIII satellites with respective bond energies around 786 and 803 eV correspond to Co^{3+}, Co^{2+}, and the paramagnetic Co^{2+} and Co^{3+} mixture [20]. High proportion of Co^{2+} in the tetrahedral sites are observed by comparison to Co^{3+} content in octahedral sites. This is beneficial for OER activity, which depends on the relative surface ratio of Co^{2+}/Co^{3+}. Co^{2+} ions induce the formation of cobalt oxyhydroxide (Co-OOH), which enhance OER activity [16,17]. In contrast, the Co^{3+} ions are detrimental for OER activity because they contribute to strength the adsorption of hydroxides groups at the electrocatalysts surface [21].

The Cu 2p 3/2 core-level spectrum is presented in Figure 4 and data related to the deconvolved peaks are shown in Table 3. The Cu 2p 3/2 core-level spectrum shows one peak at ~ 933 eV and an intense satellite peak at ~ 941 eV. The deconvolution of the main peak shows the presence of two components: i) the first one with a binding energy close to 930 eV, corresponding to Cu^+ in tetrahedral sites, and ii) the second one with a binding energy close to 933 eV, corresponding to Cu^{2+} in octahedral sites [20,22]. The presence of Cu^{2+} can induce good intrinsic performance of the electrocatalyst for ORR, because they are active oxygen adsorption sites [23].

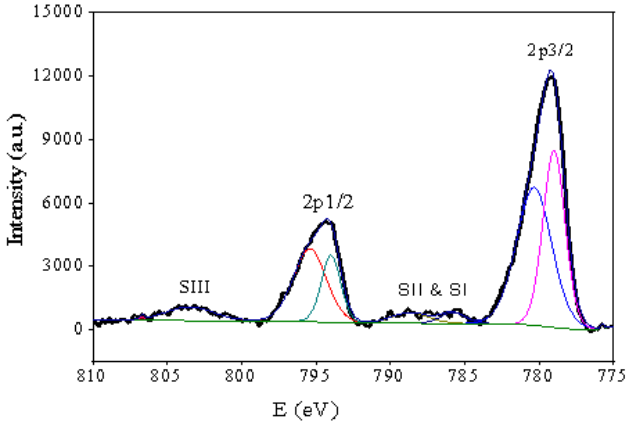

Figure 3. Co 2p core-level spectrum of catalyst prepared by nanocasting and annealed at 350 °C under atmosphere and air conditions

Table 2. Data related to Co 2p core-level spectrum of electrocatalyst powders prepared by nanocasting and annealed at 350 °C

Co^{2+} (tetrahedral sites)			Co^{3+} (octahedral sites)		
BE (eV)	FWHM (eV)	Relative surface area (%)	BE (eV)	FWHM (ev)	Relative surface area (%)
780.35	2.80	55.78	779.01	1.74	44.21

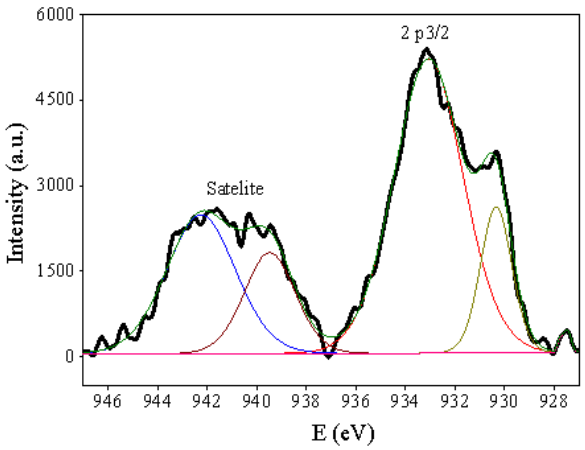

Figure 4. Cu 2 p3/2 core-level spectrum annealed of catalyst prepared by nanocasting and annealed at 350 °C under atmosphere and air conditions

Table 3. Data related to Cu 2p core-level spectrum of electrocatalyst powders prepared by nanocasting and annealed at 350 °C

Cu^{2+} (octahedral sites)			Cu^{+} (tetrahedral sites)		
BE (eV)	FWHM (eV)	Relative Surface area (%)	BE (eV)	FWHM (ev)	Relative Surface area (%)
933	3.28	81.60	930	1.49	18.40

Mn 2p 3/2 and Mn 2p 1/2 core-level spectrum is presented in Figure 5 and data related to the deconvolved peaks are shown in Table 4. The spectrum shows two peaks and the deconvolution of each peaks gives two components: i) Mn^{3+} in tetrahedral sites (BE~ 641, 655 eV), and ii) Mn^{4+} ions in the octahedral sites (BE~ 643, 652eV) [24]. From Table 4, the predominance of Mn^{4+} ions compared to Mn^{3+} ions in the octahedral sites favor ORR can be seen. Mn^{4+} ions plays an essential role in electrocatalysis, particularly for the ORR, because they are adsorption site [25].

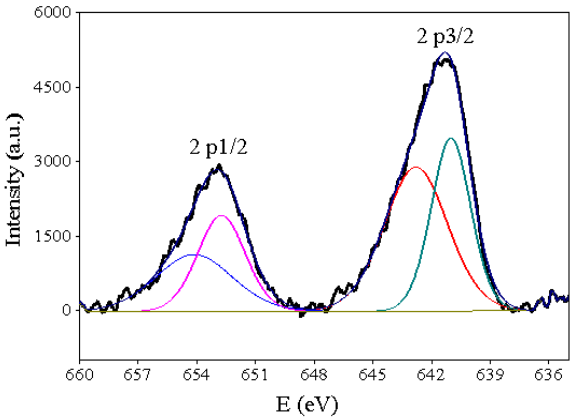

Figure 5. Mn 2 p core-level spectrum annealed of catalyst prepared by nanocasting and annealed at 350 °C under atmosphere and air conditions

The O 1s spectrum is presented in Figure 6 and data related to the deconvolved peaks are shown in Table 5. The O 1s spectrum fitted into three types of oxygen contributions. The main component (O_I), with a binding energy close to 528 eV, is characteristic of the metal-oxygen bond and correspond to the Co-O, Mn-O and Cu-O [26,27] bonds. The second contribution (O_{II}) with binding energy close to 530 eV, is typical of oxygen in OH^{26} group from hydroxyl species such as CoOOH, MnOOH and CuOOH. The third component (O_{III}) with an binding energy close to 536 eV, corresponds to the H-O-H bond of water molecule from the environment adsorbed on the surface of the samples [26,28]. The abundance of Mn^{4+} could explained the increase in the proportion of oxygen O_I, essentially caused by Mn-OOH bonds [26].

Table 4. Data related to Mn 2p core-level spectrum of electrocatalyst powder prepared by nanocasting and annealed at 350 °C

Mn^{4+} (octahedral sites)			Mn^{3+} (tetrahedral sites)		
BE (eV)	FWHM (eV)	Relative Surface area (%)	BE (eV)	FWHM (ev)	Relative Surface area (%)
643	3.82	57.61	641	2.37	42.38

Table 5. Data related to O 1s core-level spectrum of electrocatalyst powders prepared by nanocasting and annealed at 350 °C

O_I			O_{II}			O_{III}		
BE (eV)	FWHM (eV)	Relative Surface area (%)	BE (eV)	FWHM (eV)	Relative Surface area (%)	BE (eV)	FWHM (eV)	Relative Surface area (%)
528.95	1.39	54.24	530.53	2.45	41.66	536.31	2.78	4.08

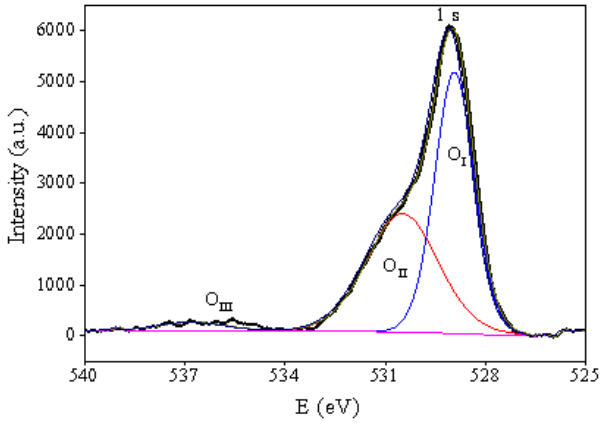

Figure 6. O 1s core-level spectrum of catalyst prepared by nanocasting and annealed at 350 °C under atmosphere and air conditions

3.2. Physicochemical Characterization of $Mn_{0.6}Cu_{0.4}Co_2O_4$ Electrocatalyst

The XRD patterns of $Mn_{0,6}Cu_{0,4}Co_2O_4$ powder are shown in Figure 7. All the diffraction peaks at 21.97°, 36.29°, 42.88°, 52.41°, 69.91° and 77.36° were indexed to the crystal plane (111), (220), (311), (400), (422) and (511) of spinel (JCPDS #18-0408). No trace of impurity phase was observed and samples from solgel and nanocasting methods show good crystallinity after calcination at 350°C. The crystallites sizes calculated using Debye Scherrer formula on the main peak (311), confirms large crystallites of about 8 nm.

Adsorption – desorption isotherms at 77 K, as well as the pores size distributions of $Mn_{0.6}Cu_{0.4}Co_2O_4$ electrocatalyst powders are presented in Figure 8. According to the IUPAC classification, all of samples have IV-type isotherms with a H4 hysteresis loop associated to adsorption in mesoporous [29]. The adsorption isotherms showed no knee point and slight adsorption in low relative pressure region (< 0.3 P/Po). This revealed a weak interaction between adsorbent and adsorbate. At relative pressure of 0.4 P/Po, N_2 adsorption begins in the mesoporous of the oxide. This is similar to value 0.43 P/Po recorded in the literature on the beginning of N_2 desorption as absorbate[30]. The increased of P/Po with the adsorption volume suggest that most of the pores of the adsorbent were filled by capillary condensation. The range of 0.4 to 1 corresponds to mesopore filling and the greatest amount of nitrogen was adsorbed between 0.8 and 1 P/Po. The drop of adsorbed nitrogen around 1 P/Po conferred the adsorption of N_2 on the external surface of the sample due to the lack of empty mesoporous. The mesoporous structure favors good electrocatalytic properties, due to the improved diffusion of electroactive species in the mesoporous, which induce large contact surface with the catalytic sites [29,31].

The pore size distribution of catalysts powders obtained by two methods (solgel and nanocasting) is presented in Figure 9. Pore sizes, pore volumes and specific surface areas are presented in Table 6. Pore size distribution was analysed on basis of isotherms adsorption. For solgel synthesis route, the pore size distribution showed a wide mesoporous size distribution between 3 and 35 nm, an average pores volume of 0.27 cm^3/g. For the nanocasting synthesis route, the KIT6-100 contributed to obtain uniform pore sized distribution of 6 nm. The average pore volume was found to be 0.18 cm^3/g. The drop in pore volume could be explained by the structuring of the oxide porosity in the nanocasting synthesis route. These results agree with those reported in literature related to materials synthetized by nanocasting route [32,33,34,35].

From the BET theory measurement, the specific surface areas were found to be 132 m^2/g and 91 m^2/g, respectively for nanocasting route and solgel method. The high surface area of nanocasting route catalyst can be attributed to the mesostructuring induced by KIT6-100 used as template in the preparation process [13]. The specific surface area is an essential parameter for electrode materials because of adsorption process involving in electrochemical activities. Lagest specific surface area leads to greater contact with the active sites of the electocatalyst [36].

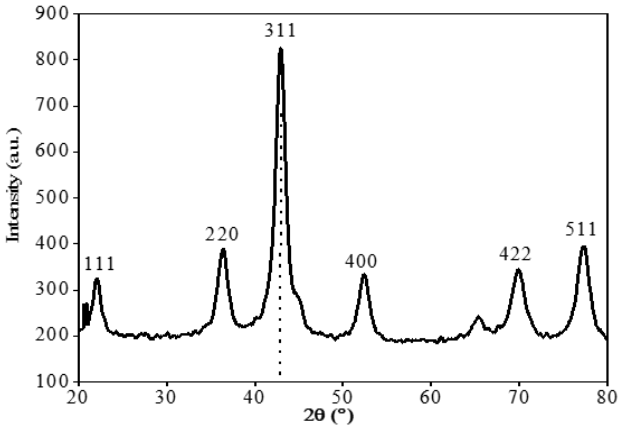

Figure 7. (a) X-ray diffraction pattern of $Mn_{0.6}Cu_{0.4}Co_2O_4$ powders prepared by nanocasting route and annealed at 350 °C under atmosphere and air conditions

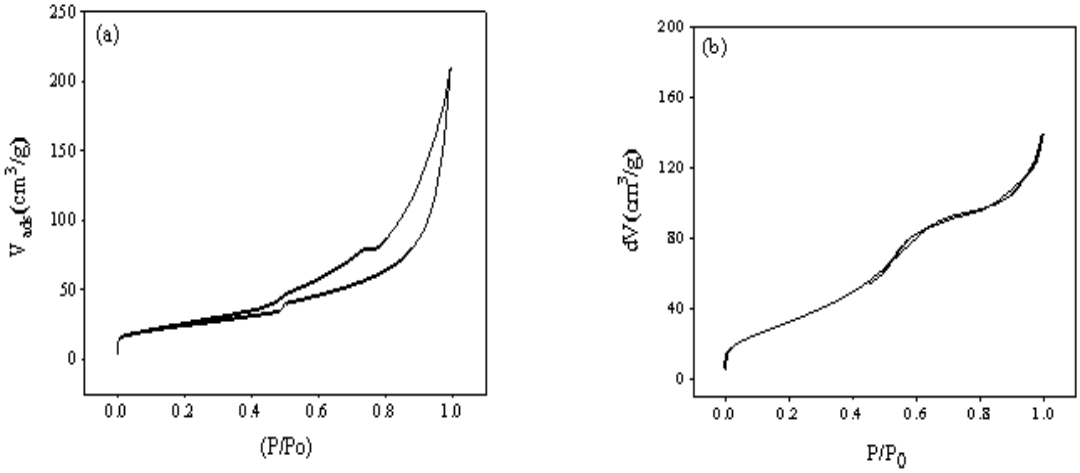

Figure 8. Adsorption-desorption isotherms: (a) solgel catalyst, (b) nanocasting catalyst. Catalyst powders were annealed at 350 °C under atmosphere and air conditions

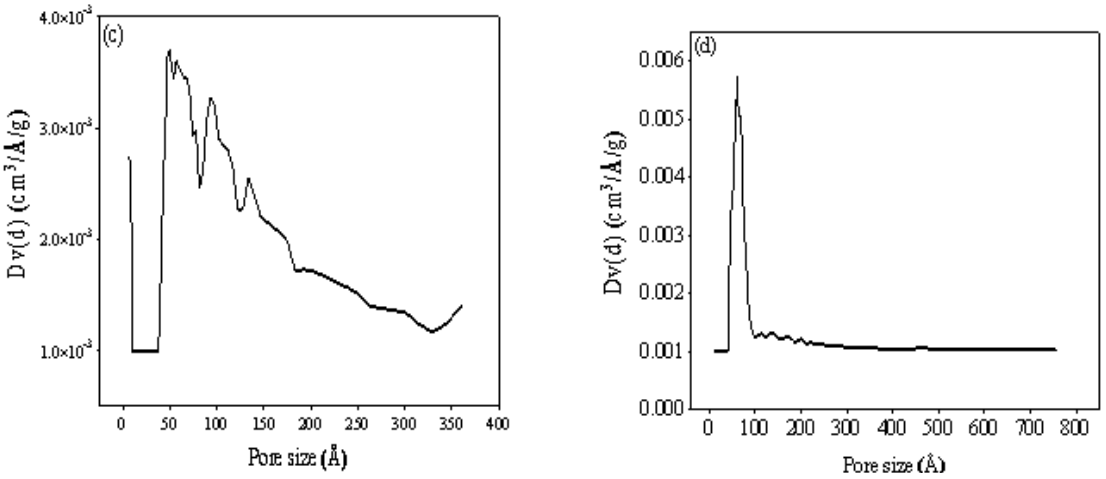

Figure 9. Pore sized distribution: (a) solgel catalyst, (b) nanocasting catalyst. Catalyst powders were annealed at 350 °C under atmosphere and air conditions

Table 6. Pore sizes and specific surface areas of electrocatalyst powders prepared by solgel and nanocasting methods and annealed at 350 °C under atmosphere and air conditions

Synthesis route	specific surface area (m^2/g)	average pore volume (cm^3/g)	average pore size (nm)
Solgel	91	0.27	2-50
Nanocasting	132	0.18	6.1

4. Conclusion

$Mn_{0.6}Cu_{0.4}Co_2O_4$ catalyst powders were successfully synthetized using two different methods: sol-gel and nanocasting. Chemical characterization of the catalyst powders did not shown significant difference between nanocasting route and sol gel method. Indeed, XRD measurements revealed that $Mn_{0.6}Cu_{0.4}Co_2O_4$ particles have good crystallinity with crystallite size of 8 nm. No secondary phase such as CuO have been found, which is detrimental to the performance of bifunctional oxygen reaction electrodes. XPS analysis revealed a predominant of tetrahedral Co^{2+}, octahedral Cu^{2+} and octahedral Mn^{4+} species at the surface compared to octahedral Co^{3+}, tetrahedral Cu^{+} and tetrahedral Mn^{3+} that beneficial for good intrinsic performance of electrocatalysts for ORR and OER. Physicochemical characterization demonstrated that nanocasting process induce higher oxide specific surface areas with BET surface value of 132 m^2/g compared to 91 m^2/g obtained by the classic solgel method. This is due to the significant decrease of the oxide mesopore volume from 0.27 to 0.18 cm^3/g and the structuring of the oxide porosity. The uniform and controlled pore size contributed to effective penetration of the liquid electrolyte.

References

[1] Jaramillo, D.; Alvarez, G.; Díaz, C.; Pérez, S.; Saldaña, J. M.; Sierra, L.; López, B. L.; Moreno-Zuria, A.; Mohamedi, M.; Palacio, R. Porous Carbonaceous Materials Simultaneously Dispersing N, Fe and Co as Bifunctional Catalysts for the ORR and OER: Electrochemical Performance in a Prototype of a Zn–Air Battery. *Dalton Transactions* **2024**, *53* (7), 3143–3158.

[2] Ran, Y.; Xu, C.; Ji, D.; Zhao, H.; Li, L.; Lei, Y. Research Progress of Transition Metal Compounds as Bifunctional Catalysts for Zinc-Air Batteries. *Nano Res. Energy* **2024**, *3*, e9120092.

[3] Zhang, X.; Wang, L.; Fu, H. Recent Advances in Rechargeable Zn-Based Batteries. *Journal of Power Sources* **2021**, *493*, 229677.

[4] Guo, Y.-F.; Zhao, S.; Zhang, N.; Liu, Z.; Wang, P.-F.; Zhang, J.; Xie, Y.; Yi, T.-F. Advanced Design Strategies for Fe-Based Metal-Organic Frameworks-Derived Electrocatalysts toward High-Performance Zn-Air Batteries. *Energy & Environmental Science* **2024**.

[5] Lakhan, M. N.; Hanan, A.; Shar, A. H.; Ali, I.; Wang, Y.; Ahmed, M.; Aftab, U.; Sun, H.; Arandiyan, H. Transition Metals-Based Electrocatalysts for Alkaline Overall Water Splitting: Advancements, Challenges, and Perspectives. *Chemical Communications* **2024**.

[6] Zhao, Q.; Yan, Z.; Chen, C.; Chen, J. Spinels: Controlled Preparation, Oxygen Reduction/Evolution Reaction Application, and Beyond. *Chemical reviews* **2017**, *117* (15), 10121–10211.

[7] Li, S.; Hao, X.; Abudula, A.; Guan, G. Nanostructured Co-Based Bifunctional Electrocatalysts for Energy Conversion and Storage: Current Status and Perspectives. *Journal of Materials Chemistry A* **2019**, *7* (32), 18674–18707.

[8] De Koninck, M.; Marsan, B. $Mn_xCu_{1-x}Co_2O_4$ Used as Bifunctional Electrocatalyst in Alkaline Medium. *Electrochimica Acta* **2008**, *53* (23), 7012–7021.

[9] De Koninck, M.; Poirier, S.-C.; Marsan, B. $Cu_xCo_{3-x}O_4$ Used as Bifunctional Electrocatalyst: Physicochemical Properties and Electrochemical Characterization for the Oxygen Evolution Reaction. *Journal of The Electrochemical Society* **2006**, *153* (11), A2103.

[10] De Koninck, M.; Poirier, S.-C.; Marsan, B. $Cu_xCo_{3-x}O_4$ Used as Bifunctional Electrocatalyst: II. Electrochemical Characterization for the Oxygen Reduction Reaction. *Journal of The Electrochemical Society* **2007**, *154* (4), A381.

[11] Kleitz, F.; Hei Choi, S.; Ryoo, R. Cubic Ia$_3$d Large Mesoporous Silica: Synthesis and Replication to Platinum Nanowires, Carbon Nanorods and Carbon NanotubesElectronic Supplementary Information (ESI) Available: TEM Images of Mesoporous Cubic Silica and Pt Networks, XRD Patterns during Forma. *Chemical Communications* **2003**, No. 17, 2136.

[12] Li, Z.; Hou, B.; Xu, Y.; Wu, D.; Sun, Y.; Hu, W.; Deng, F. Comparative Study of Solgel-Hydrothermal and Solgel Synthesis of Titania–Silica Composite Nanoparticles. *Journal of Solid State Chemistry* **2005**, *178* (5), 1395–1405.

[13] Rumplecker, A. Host-Guest Chemistry of Mesoscopically Ordered Porous Materials. *Ruhr University Bochum*, **2007**.

[14] Kirsanova, M. A.; Okatenko, V. D.; Aksyonov, D. A.; Forslund, R. P.; Mefford, J. T.; Stevenson, K. J.; Abakumov, A. M. Bifunctional OER/ORR Catalytic Activity in the Tetrahedral $YBaCo_4O_{7.3}$ Oxide. *Journal of Materials Chemistry A* **2019**, *7* (1), 330–341.

[15] Zan, L.; Amin, H. M. A.; Mostafa, E.; Abd-El-Latif, A. A.; Iqbal, S.; Baltruschat, H. Electrodeposited Cobalt Nanosheets on Smooth Silver as a Bifunctional Catalyst for OER and ORR: In Situ Structural and Catalytic Characterization. *ACS Applied Materials & Interfaces* **2022**, *14* (50), 55458–55470.

[16] Wang, H.-Y.; Hung, S.-F.; Chen, H.-Y.; Chan, T.-S.; Chen, H. M.; Liu, B. In Operando Identification of Geometrical-Site-Dependent Water Oxidation Activity of Spinel Co_3O_4. *Journal of the American Chemical Society* **2016**, *138* (1), 36–39.

[17] Wang, W.; Kuai, L.; Cao, W.; Huttula, M.; Ollikkala, S.; Ahopelto, T.; Honkanen, A.; Huotari, S.; Yu, M.; Geng, B. Mass-production of Mesoporous $MnCo_2O_4$ Spinels with Manganese (IV)-and Cobalt (II)-rich Surfaces for Superior Bifunctional Oxygen Electrocatalysis. *Angewandte Chemie* **2017**, *129* (47), 15173–15177.

[18] Gautier, J. L., Trollund, E., Ríos, E., Nkeng, P., Poillerat, G.. Characterization of thin $CuCo_2O_4$ films prepared by chemical spray pyrolysis. Study of their electrochemical stability by ex situ spectroscopic analysis. *Journal of Electroanalytical Chemistry*, **1997,** *428(1-2)*, 47-56.

[19] Gautier, J. L., Rios, E., Gracia, M., Marco, J. F., Gancedo, J. R. Characterisation by X-ray photoelectron spectroscopy of thin $Mn_xCo_{3-x}O_4$ ($1 \geq x \geq 0$) spinel films prepared by low-temperature spray pyrolysis. *Thin Solid Films*, **1997**, *311(1-2)*, 51-57.

[20] De Koninck, M.. *PhD, University of Québec*; Montréal, **2007**.

[21] Kim, M. S.; Lim, E.; Kim, S.; Jo, C.; Chun, J.; Lee, J. General Synthesis of N‐Doped Macroporous Graphene‐Encapsulated Mesoporous Metal Oxides and Their Application as New Anode Materials for Sodium‐Ion Hybrid Supercapacitors. *Advanced Functional Materials* **2017**, *27* (3), 1603921.

[22] Zhao, H.; Zhou, X. X.; Pan, L. Y.; Wang, M.; Chen, H. R.; Shi, J. L. Facile Synthesis of Spinel $Cu_{1.5}Mn_{1.5}O_4$ Microspheres with High Activity for the Catalytic Combustion of Diesel Soot. *RSC Advances* **2017**, *7* (33), 20451–20459.

[23] Nabae, Y.; I. Yamanaka; Otsuka, K. No Title. *Appl. Catal. A*, **2005,** *280, 149*.

[24] Wu, M.; Zhang, L.; Gao, J.; Zhou, Y.; Zhang, S.; Chen, A. Facile Conversion of the Surface Layers of Graphite to Capacitive Manganese Oxide Coatings. *Journal of The Electrochemical Society* **2008**, *155* (5), A355.

[25] Strohmeier, R.; Brian, H.; David, M. Surf Ace Spectroscopic Characterization of Mn/AI,O, Catalysts. **1984**, *9*, 4922–4929.

[26] Jiang, H., Ma, J., Li, C., Hierarchical porous $NiCo_2O_4$ nanowires for high-rate supercapacitors. *Chemical communications*, **2012,** *48(37)*, 4465-4467.

[27] Ruan, M.; Wei, X.; Chen, H.; Wang, L.; Li, T.; Wang, H.; Yang, D.; Guo, M. Promotion of Oxygen Evolution through the Modification of Co-O Bond in Spinel $NiCo_2O_4$. *Journal of Physics and Chemistry of Solids* **2024**, *189*, 111955.

[28] Rebekah, A.; Kumar, E. A.; Viswanathan, C.; Ponpandian, N. Effect of Cation Substitution in $MnCo_2O_4$ Spinel Anchored over RGO for Enhancing the Electrocatalytic Activity towards Oxygen Evolution Reaction (OER). *International Journal of Hydrogen Energy* **2020**, *45* (11), 6391–6403.

[29] Tsai, C.-C.; Teng, H. Regulation of the Physical Characteristics of Titania Nanotube Aggregates Synthesized from Hydrothermal Treatment. *Chemistry of Materials* **2004**, *16* (22), 4352–4358.

[30] Lafont, M. U., PhD, National School of Chemistry, University of Montpellier, **2003**.

[31] Cao, L.; Lu, M.; Li, H. L. Preparation of mesoporous nanocrystalline Co_3O_4 and its applicability of porosity to the formation of electrochemical capacitance. *J. Electrochem. Soc.***(2005)** *152, A871*.

[32] Cabo, M.; Pellicer, E.; Rossinyol, E.; Solsona, P.; Castell, O.; Suriñach, S.; Baró, M. D. Influence of the Preparation Method on the Morphology of Templated $NiCo_2O_4$ Spinel. *Journal of Nanoparticle Research* **2011**, *13*, 3671–3681.

[33] Grewe, T.; Deng, X.; Tüysüz, H. Influence of Fe Doping on Structure and Water Oxidation Activity of Nanocast Co3O4. *Chemistry of materials* **2014**, 26 (10), 3162–3168.

[34] Abidat, I.; Bouchenafa-Saib, N.; Habrioux, A.; Comminges, C.; Canaff, C.; Rousseau, J.; Napporn, T. W.; Dambournet, D.; Borkiewicz, O.; Kokoh, K. B. Electrochemically Induced Surface Modifications of Mesoporous Spinels ($Co_3O_{4-\delta}$, $MnCo_2O_{4-\delta}$, $NiCo_2O_{4-\delta}$) as the Origin of the OER Activity and Stability in Alkaline Medium. *Journal of Materials Chemistry A* **2015**, *3 (33)*, 17433–17444.

[35] Cabo, M.; Pellicer, E.; Rossinyol, E.; Estrader, M.; López-Ortega, A.; Nogués, J.; Castell, O.; Suriñach, S.; Baró, M. D. Synthesis of Compositionally Graded Nanocast $NiO/NiCo_2O_4/Co_3O_4$ Mesoporous Composites with Tunable Magnetic Properties. *Journal of Materials Chemistry* **2010**, *20 (33)*, 7021–7028.

[36] Zhou, S.; Shi, H.; Feng, X.; Xue, K.; Song, W. Design of Templated Nanoporous Carbon Electrode Materials with Substantial High Specific Surface Area for Simultaneous Determination Ofbiomolecules. *Biosensors and Bioelectronics* **2013**, *42*, 163–169.